ACS APPLIED MATERIALS & INTERFACES
Research Article
www.acsami.org

Photocurrent Response of MoS_2 Field-Effect Transistor by Deep Ultraviolet Light in Atmospheric and N_2 Gas Environments

M. F. Khan,[†] M. W. Iqbal,[†] M. Z. Iqbal,[†] M. A. Shehzad,[‡] Y. Seo,[‡] and Jonghwa Eom*,[†]

[†]Department of Physics and Graphene Research Institute and [‡]Faculty of Nanotechnology & Advanced Materials Engineering and Graphene Research Institute, Sejong University, Seoul 143-747, Korea

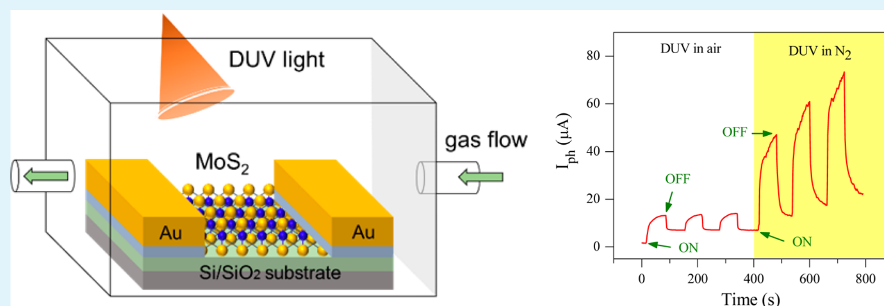

ABSTRACT: Molybdenum disulfide (MoS_2), which is one of the representative transition metal dichalcogenides, can be made as an atomically thin layer while preserving its semiconducting characteristics. We fabricated single-, bi-, and multilayer MoS_2 field-effect transistor (FET) by the mechanical exfoliation method and studied the effect of deep ultraviolet (DUV) light illumination. The thickness of the MoS_2 layers was determined using an optical microscope and further confirmed by Raman spectroscopy and atomic force microscopy. The MoS_2 FETs with different number of layers were assessed for DUV-sensitive performances in various environments. The photocurrent response to DUV light becomes larger with increasing numbers of MoS_2 layers and is significantly enhanced in N_2 gas environment compared with that in atmospheric environment.

KEYWORDS: *MoS_2, transition metal dichalcogenides, electrical measurement, deep ultraviolet light, photocurrent response*

1. INTRODUCTION

Two-dimensional (2D) materials have facilitated new possibilities for electronic materials. For example, graphene is an appealing 2D material that has significant potential for application in electronic materials because of its superior electrical, photoelectrical, and biosensing properties.[1] However, graphene is a gapless material that has limitations in photodetecting and switching device applications. Transition metal dichalcogenide (TMDC) is an alternative material that has attractive properties, such as band gap and atomically thin-layered structure.[2−6] Several 2D layered materials, such as molybdenum disulfide, gallium sulfide, gallium selenide, and tungsten diselenide,[4,7−21] provide many advantages for photoelectrical devices.

MoS_2 is one of the most promising 2D TMDCs because of its layer-dependent band gap and sensitivity to surface adsorbents.[22] Multilayer (ML) MoS_2 has an indirect band gap of ~1.2 eV, whereas single-layer (SL) MoS_2 has a direct band gap of ~1.8 eV. The dependence of energy band gap to the thickness of MoS_2 layer has been examined in theoretical studies.[4,23−29] The layer-dependent light spectral response of MoS_2 sheets suggests that both ML and SL MoS_2 materials provide valuable properties for field-effect transistors (FETs).[9] One of the advantages of ML MoS_2 films is a capability of high current flow. A sufficiently high current can flow in the ballistic limit of ML MoS_2 films because the density of states in ML MoS_2 is three times higher than that in SL MoS_2.[30] The layer-dependent band gap in MoS_2 films is also useful for optoelectronics,[16,17,31−34] and a high surface-to-volume ratio is suitable for gas sensing.[35−37] Although several studies have been performed on atomically thin-layered MoS_2 devices for photocurrent response and possible gas sensing performance,[38−45] intensive investigations are still required to understand the photocurrent saturation−relaxation behavior and the effects of environments.

In this paper, we fabricated exfoliated SL, bilayer (BL), and ML MoS_2 FETs. The thickness of MoS_2 flakes was determined by optical microscopy and further confirmed by Raman spectroscopy. We investigated the electrical transport properties of MoS_2 FETs, which showed n-type semiconductor behavior. Photocurrent response was studied for different drain-source bias voltages by irradiation of a 220 nm dominant wavelength of deep ultraviolet (DUV) light. The time-dependent photocurrent response was studied for different layers of MoS_2 FETs. We also investigated the photocurrent response of MoS_2 FETs in air and nitrogen (N_2) gas environments.

Received: September 30, 2014
Accepted: November 19, 2014
Published: November 19, 2014

 © 2014 American Chemical Society dx.doi.org/10.1021/am506716a | ACS Appl. Mater. Interfaces 2014, 6, 21645−21651

2. EXPERIMENTAL SECTION

SL, BL, and ML MoS_2 flakes were obtained by mechanical exfoliation. The MoS_2 flakes were placed on p-type doped Si substrates with 300 nm-thick SiO_2 cap layer.[4,46,47] The SL, BL, and ML flakes were identified by optical microscopy, Raman spectroscopy, and atomic force microscopy (AFM). The number of layers of MoS_2 was determined using Renishaw Raman spectroscopy with laser wavelength of 514 nm. As first step of photolithography photoresist (SPR) and ethyl lactate (EL) were spin-coated on Si substrates. After developing the patterns by photolithography oxygen (O_2) plasma was applied for 5 min to remove residues of SPR and EL. The large patterns were made by evaporation of Cr/Au (10/30 nm). The fine electrode patterns were made by e-beam lithography and subsequent deposition of Cr/Au (10/60 nm) by thermal evaporation technique. Figure 1a shows a schematic view of the MoS_2 FET for photocurrent response measurement under DUV light.

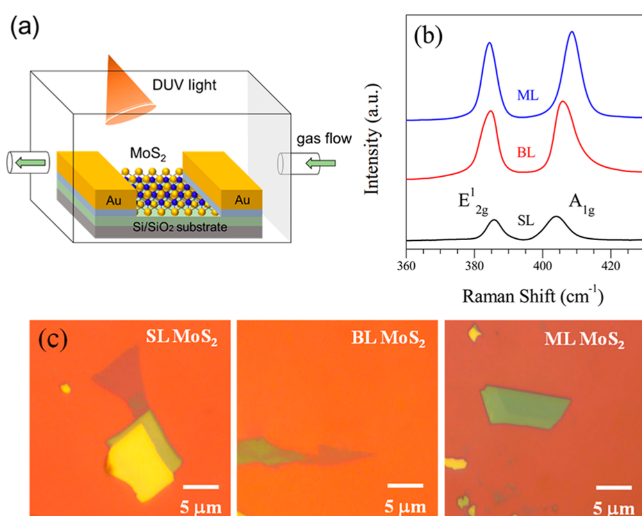

Figure 1. (a) Schematic drawing of MoS_2 FET. (b) Raman spectra of pristine SL, BL, and ML of MoS_2 flakes. (c) Optical images of SL, BL, and ML of MoS_2.

3. RESULTS AND DISCUSSION

Raman spectroscopy is a sensitive and nondestructive tool that provides accurate, plausible, and fine information on properties such as fine structure, thermal conductivity, strain effect, and chemical and impurity adsorption on material surfaces.[48−55] Vibrational properties, particularly electron−phonon interactions of MoS_2, are important for Raman spectroscopy characterization because such properties have significant effects on the performance of MoS_2 FETs. The Raman spectra of our MoS_2 layers were analyzed at room temperature by keeping the laser wavelength at 514 nm and small laser power at 1.0 mW to avoid heating effect. Figure 1b shows the Raman spectra for different layers of pristine MoS_2 flakes, and the results show the number of layers. The SL has strong bands at ∼386 and ∼404 cm^{-1}, which are attributed to in-plane vibrational (E^1_{2g}) and out-of-plane vibrational (A_{1g}) modes, respectively. When the number of layers was increased from SL to ML, the E^1_{2g} bands moved toward lower wavenumbers, whereas the A_{1g} bands moved toward higher wavenumbers. The E^1_{2g} and A_{1g} bands of BL are observed at ∼385 and ∼406 cm^{-1}, respectively. Similarly, the E^1_{2g} and A_{1g} peaks of ML are found at ∼384 and ∼408 cm^{-1}. The approximate gaps between E^1_{2g} and A_{1g} bands of SL, BL, and ML MoS_2 flakes are ∼18, ∼21, and ∼24 cm^{-1}, respectively. These observations are consistent with those of previous reports.[38,47,56] The MoS_2 layers were identified by optical images and shown in Figure 1c. The AFM images of SL, BL, and ML MoS_2 flakes are shown in Figure 2a−c, respectively. The measured thicknesses of SL, BL, and ML MoS_2 flakes are ∼0.9, 1.72, and 8 nm, respectively (Figure 2d−f, respectively); these results are also consistent with those of previous reports.[20,26]

The electrical properties of MoS_2 FETs were investigated in vacuum by applying back-gate voltage (V_g). We measured the transfer and output characteristics of SL, BL, and ML MoS_2 FETs. Figure 3a shows the transfer characteristics of SL, BL, and ML MoS_2 FETs. Transfer characteristics (drain-current I_D as a function of V_g) were measured at fixed drain-source voltage (V_{ds}) = 1 V. The I_D increased by a few orders of magnitude with increasing V_g. Figure 3b−d shows the output character-

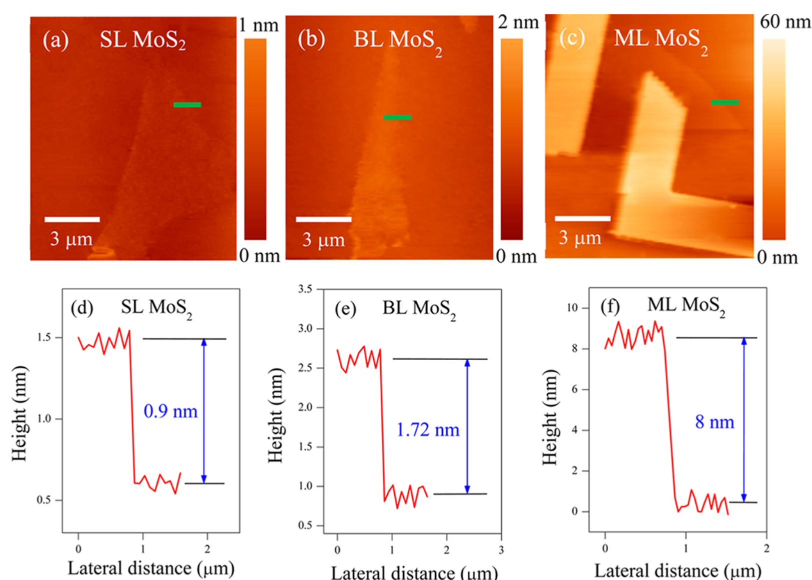

Figure 2. AFM images of (a) SL, (b) BL, and (c) ML MoS_2 flakes. Height profiles of (d) SL, (e) BL, and (f) ML MoS_2 flakes along the green lines in AFM images.

dx.doi.org/10.1021/am506716a | ACS Appl. Mater. Interfaces 2014, 6, 21645−21651

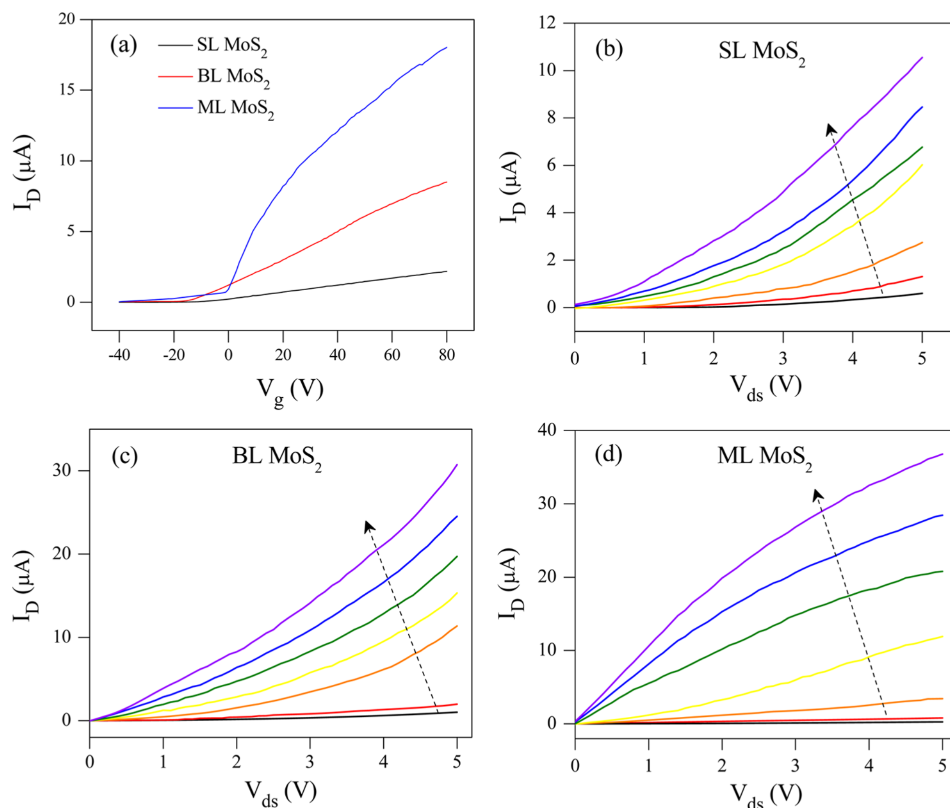

Figure 3. (a) Transfer characteristics of pristine SL, BL, and ML MoS_2 FETS. (b) Output characteristics of (b) SL, (c) BL, and (d) ML MoS_2 FETs at V_g ranging from −30 V to +30 V with change of 10 V step. All measurements were performed at room temperature in vacuum.

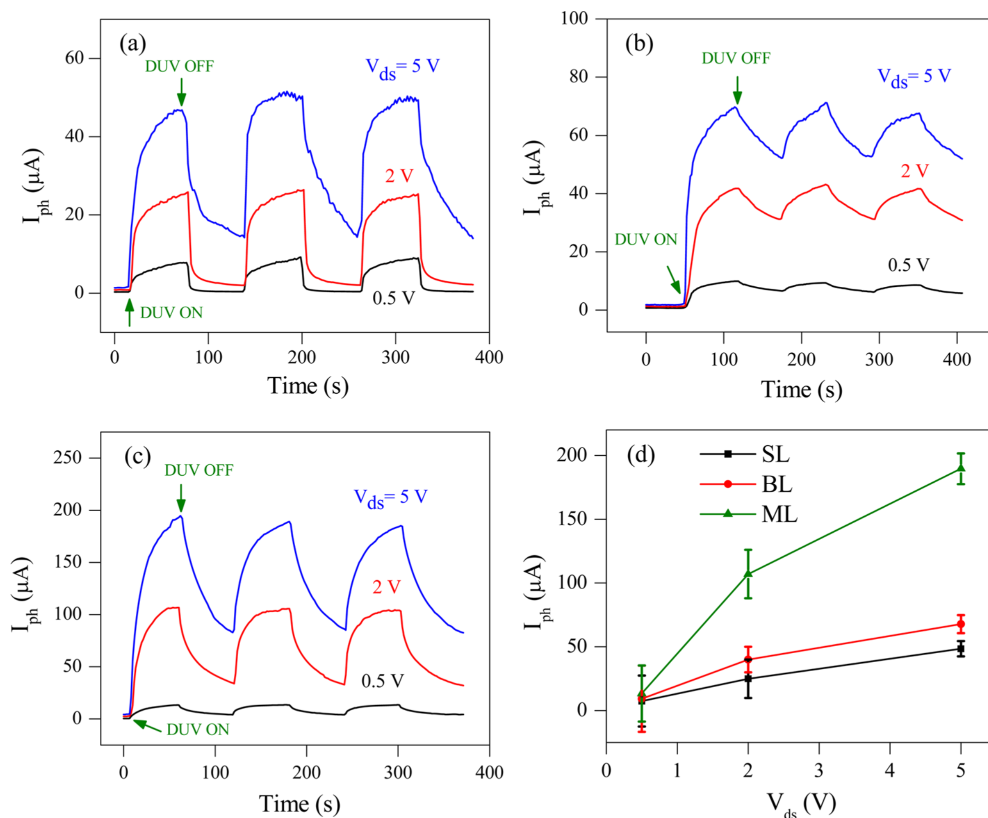

Figure 4. Photocurrent response after switching on and off the DUV light with V_{ds} of 0.5, 2.0, and 5.0 V for (a) SL, (b) BL, and (c) ML MoS_2 FETs, respectively. (d) Comparative photocurrent generation of SL, BL, and ML MoS_2 FETs as a function of V_{ds}. All measurements were performed at V_g = 0 V in atmospheric environment.

dx.doi.org/10.1021/am506716a | ACS Appl. Mater. Interfaces 2014, 6, 21645−21651

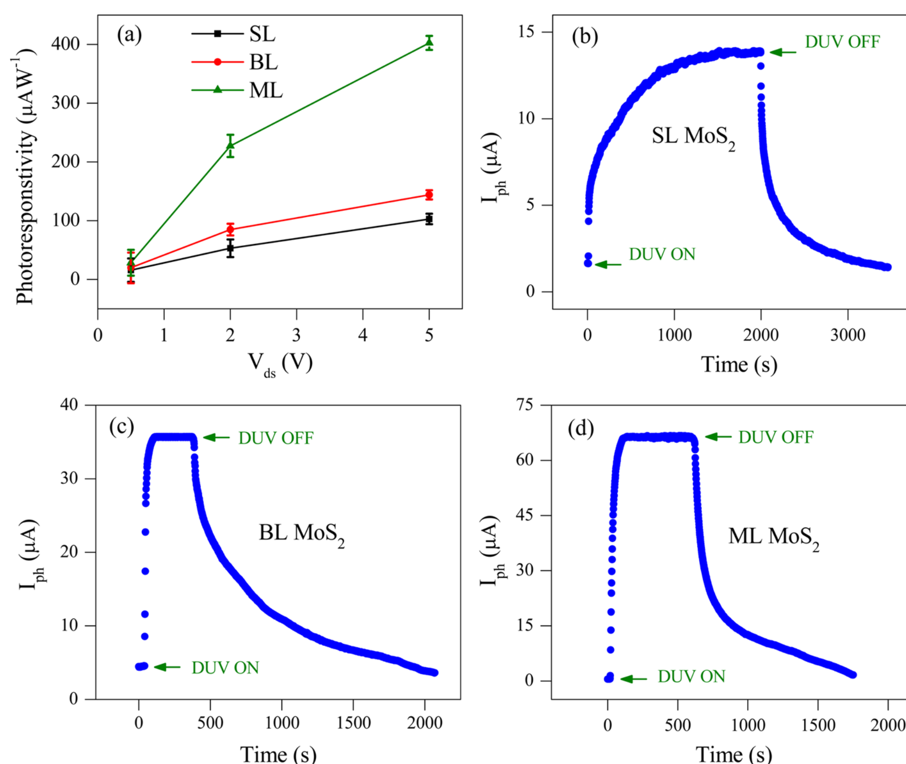

Figure 5. (a) Photoresponsivity of SL, BL, and ML MoS_2 FETs as a function of V_{ds}. Relaxation of photocurrent of (b) SL, (c) BL, and (d) ML MoS_2 FETs at V_{ds} = 1 V after switching DUV light on and off. All measurements were performed at V_g = 0 V in atmospheric environment.

istics of SL, BL, and ML MoS_2 FETs. The output characteristics (I_D vs V_{ds}) were measured at fixed V_g ranging from −30 to +30 V (bottom to top) with a step of 10 V. The V_g-dependent output characteristics of MoS_2 FETs indicate the characteristics of an n-type transistor. The field-effect mobilities of the different MoS_2 layers were obtained using $\mu = [L/(WC_gV_{ds})]$. $[(dI_{ds}/dV_g)]$, where (dI_{ds}/dV_g) is slope of linear region of transfer curves, C_g is the gate capacitance (∼115 aF/μm^2) of the Si substrate with 300 nm thick SiO_2 cap layer, V_{ds} is the drain-source current for each device, L is the channel length and W is the channel width. The mobilities of SL, BL, and ML devices are 0.8, 6, and 17 $cm^2\ V^{-1}\ s^{-1}$, respectively. The ML FET showed higher I_D and larger mobility than BL and SL FETs. The charge carrier densities (n) of MoS_2 layers were calculated by using the relation, $n = C_g(V_g - V_{th})/e$, where V_{th} is the threshold voltage of SL, BL, and ML MoS_2 devices and e is the electronic charge. The threshold voltage of SL, BL, and ML MoS_2 FETs are at −21, −20, and −8 V, respectively. The charge carrier densities of SL, BL, and ML MoS_2 devices at V_g = 30 V were 3.6×10^{12}, 3.5×10^{12}, and 2.7×10^{12} cm^{-2} respectively. The I_{on}/I_{off} ratios of SL, BL, and ML MoS_2 FETs at room temperature were found to be $\sim 1 \times 10^5$, $\sim 1 \times 10^3$, and $\sim 1 \times 10^3$, respectively.

We have investigated the hysteresis in transfer characteristics of (a) SL, (b) BL, and (c) ML MoS_2 FETs in vacuum. When V_g was swept from −40 V to +80 V, the threshold voltages of SL, BL, and ML MoS_2 devices were found around −21, −20, and −8 V respectively. However, when V_g was swept from +80 V to −40 V, the threshold voltage were found around 0, −5, and 1 V respectively. So the hysteresis in SL, BL and ML MoS_2 FETs was ∼21, ∼15, and ∼9 V, respectively. Because the charge impurities, such as oxygen molecules, can be captured at the surface of MoS_2, the surface-to-volume ratio of MoS_2 flake is an important factor to the occurrence of hysteresis in the transfer characteristics. The large hysteresis in SL MoS_2 FET is related with the large surface-to-volume ratio. The hysteresis of MoS_2 FETs in air and N_2 gas flow remains almost same as in vacuum, which indicates that charge impurities cannot be easily removed or added at the surface of MoS_2 by normal gas flow.

Figure 4a−c shows the photocurrent [$I_{ph} = I_D$(time) − I_D(initial state)] of SL, BL, and ML FETs as a function of exposure time of DUV light in atmospheric environment at different bias voltages (V_{ds} = 0.5, 2.0, 5.0 V). The intensity of DUV light was 11 mW/m^2. We kept V_g = 0 and switched the DUV light on and off for cycles of 60s each. When the DUV light was turned on, the photocurrent increased to higher values for 60s and decreased to lower values after turning off the DUV light for another 60s. The photocurrent also depends on the drain-source bias voltage applied to MoS_2 FETs. The photocurrent of SL MoS_2 FET showed I_{ph} of 7.5, 25.0, and 48.5 μA at V_{ds} of 0.5, 2.0, and 5.0 V, respectively. The photocurrent of BL MoS_2 FET showed I_{ph} of 9.3, 40.0, and 67.8 μA at V_{ds} of 0.5, 2.0, and 5.0 V, respectively. Similarly, the photocurrent of ML MoS_2 FET showed I_{ph} of 13.4, 107.0, and 189.6 μA at V_{ds} of 0.5, 2.0, and 5.0 V, respectively. The photocurrent of ML MoS_2 FET is larger than those of SL and BL MoS_2 FETs (Figure 4d). This finding is attributed to the higher density of states and small energy band gap (∼1.29 eV) in ML MoS_2 FET.

Photodetector performance can be estimated by the responsivity of the device to light illumination.[57] Photoresponsivity is defined as photocurrent per unit area per illumination power. In this study, we measured the photoresponsivity for DUV light at 11 mW/cm^{-2} and V_g = 0 V. Figure 5a shows the photoresponsivity of SL, BL, and ML MoS_2 FETs as a function of V_{ds}. The ML MoS_2 FET showed

better photoresponsivity at ~401 μAW^{-1} than those of SL and BL MoS_2 FETs. When the V_{ds} was increased, the photocurrent and photoresponsivity also increased for all the MoS_2 FETs. The dependence of photocurrent and photoresponsivity on V_{ds} is related to charge carrier drift velocities in different V_{ds}.[58]

We examined the detailed response behavior of photocurrent by 220 nm dominant DUV light. We illuminated the MoS_2 FETs with DUV light until photocurrent was saturated as shown in Figure 5 and then turned off the DUV light to observe the photocurrent decaying behavior. The saturation photocurrents of SL, BL, and ML MoS_2 FETs are ~14, ~36, and ~66 μA at V_{ds} = 1 V and V_g = 0 V (Figure 5b–d, respectively). The photocurrent decaying behavior of SL, BL, and ML MoS_2 FETs is shown in Figure 6a–c, respectively. The photocurrent decaying measurements were performed at ambient condition. The decaying behavior of SL, BL, and ML MoS_2 FETs are fitted using the stretched-exponential function:[38,59]

$$I_{ph}(t) = I_{ph}(0)\exp[-(t/\tau)^{\beta}] \quad (1)$$

where $I_{ph}(0)$ is the photocurrent when the DUV light is switched off, τ is the relaxation time, and β is the exponent that reflects the relaxation mechanism. The time constants of SL, BL, and ML MoS_2 FETs are 59, 49, and 29 s, respectively. The black solid circles show the experimental data, and the red line shows the result fitted by eq 1. The relaxation time of SL MoS_2 FET is larger than that of ML MoS_2 FET according to band gap size. Defects and impurities can induce extra energy levels inside the energy band gap, which affects the relaxation behavior. However, the observed relaxation time shows a consistent dependence on the number of layers in MoS_2 FETs, which suggests that the main mechanism of photocurrent relaxation is closely related to the energy gap of the MoS_2 layer.

The environmental effect of photocurrent response of MoS_2 FETs was investigated to assess the performance of these devices as DUV light detectors (see Figure 7). We measured the photocurrent while the SL, BL, and ML MoS_2 FETs were illuminated by DUV light in atmospheric and N_2 gas environments at room temperature. The measurement was performed at V_{ds} = 1 V and V_g = 0 V. We observed more enhancement of photocurrent generation in the N_2 gas environment compared with that in atmospheric environment. This observation is ascribed to the presence of oxygen in the air, which affects the charge-carrier density of MoS_2 layers.[60,61] The enhancement of photocurrent response in N_2 gas environment is more dominant for SL MoS_2 FET. This finding is attributed to the higher surface-to-volume ratio than that of BL and ML MoS_2 FETs.

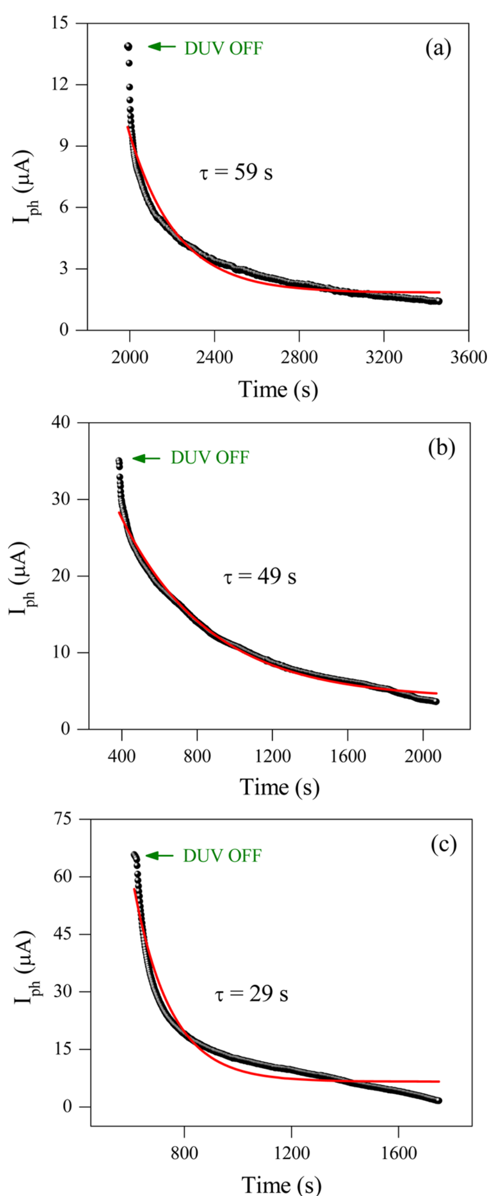

Figure 6. Photocurrent relaxation of (a) SL, (b) BL, and (c) ML MoS_2 FETs with V_{ds} = 1 V after switching DUV light off in atmospheric environment. Red curves are results fitted by eq 1

4. CONCLUSION

We fabricated SL, BL, and ML MoS_2 FETs. The MoS_2 flakes obtained via mechanical exfoliation were identified using an optical microscope and further confirmed by Raman spectroscopy and AFM. The electrical properties of SL, BL, and ML MoS_2 FETs were examined in vacuum. The ML MoS_2 FET had higher I_D and larger mobility than BL and SL MoS_2 FETs. The photocurrent responses of SL, BL, and ML MoS_2 FETs were studied using 220 nm dominant DUV light at V_g = 0 V. The photocurrent was proportional to the drain-source bias voltage, which was applied to the devices. The ML MoS_2 FET showed larger photocurrent than SL and BL MoS_2 FETs because of its small band gap and higher density of states. The relaxation of photocurrent response after turning off the DUV light was also studied for SL, BL, and ML MoS_2 FETs. The relaxation time of ML MoS_2 FET was shorter than those of SL and BL MoS_2 FETs, which was attributed to the size of energy band gap. The environmental effect of the photocurrent response of MoS_2 FETs was investigated to compare device performances in atmospheric and N_2 gas environments. The photocurrent generation was enhanced for MoS_2 FETs in the N_2 gas environment compared with that in the atmospheric environment. The sensitivity of photocurrent response in N_2 gas environment was prominent for SL MoS_2 FET compared with those for BL or ML MoS_2 FET. The surface-to-volume ratio could have a crucial effect in determining the dependence of environmental effect.

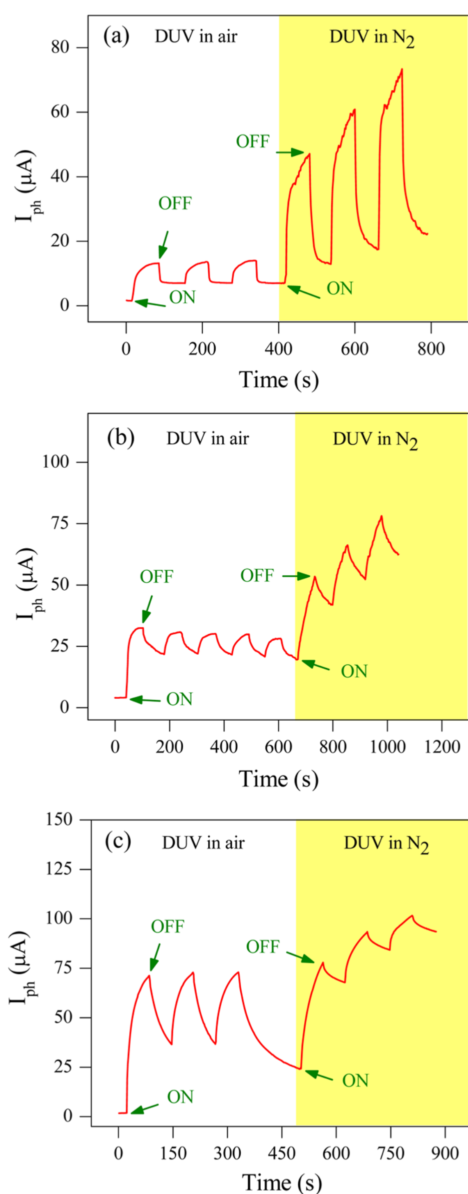

Figure 7. Photocurrent response in atmospheric and N_2 environments after switching DUV light on and off for (a) SL, (b) BL, and (c) ML MoS_2 FETs. All measurements were performed at V_{ds} = 1 V.

AUTHOR INFORMATION

Corresponding Author

*E-mail: eom@sejong.ac.kr.

Notes

The authors declare no competing financial interest.

ACKNOWLEDGMENTS

This research was supported by Nano-Material Technology Development Program (2012M3A7B4049888) through the National Research Foundation of Korea (NRF) funded by the Ministry of Science, ICT and Future Planning. This research was also supported by Priority Research Center Program (2010-0020207) and the Basic Science Research Program (2013R1A1A2061396) through NRF funded by the Ministry of Education.

REFERENCES

(1) Novoselov, K. S.; Fal'ko, V. I.; Colombo, L.; Gellert, P. R.; Schwab, M. G.; Kim, K. A Roadmap for Graphene. *Nature* **2012**, *490*, 192−200.

(2) Geim, A. K.; Novoselov, K. S. The Rise of Graphene. *Nat. Mater.* **2007**, *6*, 183−191.

(3) Castro Neto, A. H.; Guinea, F.; Peres, N. M. R.; Novoselov, K. S.; Geim, A. K. The Electronic Properties of Graphene. *Rev. Mod. Phys.* **2009**, *81*, 109−162.

(4) Radisavljevic, B.; Radenovic, A.; Brivio, J.; Giacometti, V.; Kis, A. Single-Layer MoS_2 Transistors. *Nat. Nanotechnol.* **2011**, *6*, 147−150.

(5) Mak, K. F.; Lee, C.; Hone, J.; Shan, J.; Heinz, T. F. Atomically Thin MoS_2: A New Direct-Gap Semiconductor. *Phys. Rev. Lett.* **2010**, *105*, 136805.

(6) Wang, Q. H.; Kalantar-Zadeh, K.; Kis, A.; Coleman, J. N.; Strano, M. S. Electronics and Optoelectronics of Two-Dimensional Transition Metal Dichalcogenides. *Nat. Nanotechnol.* **2012**, *7*, 699−712.

(7) Wang, H.; Yu, L. L.; Lee, Y. H.; Shi, Y. M.; Hsu, A.; Chin, M. L.; Li, L. J.; Dubey, M.; Kong, J.; Palacios, T. Integrated Circuits Based on Bilayer MoS_2 Transistors. *Nano Lett.* **2012**, *12*, 4674−4680.

(8) Jariwala, D.; Sangwan, V. K.; Late, D. J.; Johns, J. E.; Dravid, V. P.; Marks, T. J.; Lauhon, L. J.; Hersam, M. C. Band-Like Transport in High Mobility Unencapsulated Single-Layer MoS_2 Transistors. *Appl. Phys. Lett.* **2013**, *102*, 173107.

(9) Kim, S.; Konar, A.; Hwang, W. S.; Lee, J. H.; Lee, J.; Yang, J.; Jung, C.; Kim, H.; Yoo, J. B.; Choi, J. Y.; Jin, Y. W.; Lee, S. Y.; Jena, D.; Choi, W.; Kim, K. High-Mobility and Low-Power Thin-Film Transistors Based on Multilayer MoS_2 crystals. *Nat. Commun.* **2012**, *3*, 1011.

(10) Matte, H. S. S. R.; Gomathi, A.; Manna, A. K.; Late, D. J.; Datta, R.; Pati, S. K.; Rao, C. N. R. MoS_2 and WS_2 Analogues of Graphene. *Angew. Chem., Int. Ed.* **2010**, *49*, 4059−4062.

(11) Yin, Z. Y.; Li, H.; Li, H.; Jiang, L.; Shi, Y. M.; Sun, Y. H.; Lu, G.; Zhang, Q.; Chen, X. D.; Zhang, H. Single-Layer MoS_2 Phototransistors. *ACS Nano* **2012**, *6*, 74−80.

(12) Ayari, A.; Cobas, E.; Ogundadegbe, O.; Fuhrer, M. S. Realization and Electrical Characterization of Ultrathin Crystals of Layered Transition-Metal Dichalcogenides. *J. Appl. Phys.* **2007**, *101*, 14507.

(13) Ghatak, S.; Pal, A. N.; Ghosh, A. Nature of Electronic States in Atomically Thin MoS_2 Field-Effect Transistors. *ACS Nano* **2011**, *5*, 7707−7712.

(14) Late, D. J.; Liu, B.; Matte, H. S. S. R.; Dravid, V. P.; Rao, C. N. R. Hysteresis in Single-Layer MoS_2 Field Effect Transistors. *ACS Nano* **2012**, *6*, 5635−5641.

(15) Castellanos-Gomez, A.; Agrait, N.; Rubio-Bollinger, G. Optical Identification of Atomically Thin Dichalcogenide Crystals. *Appl. Phys. Lett.* **2010**, *96*, 213116.

(16) Kashid, R. V.; Late, D. J.; Chou, S. S.; Huang, Y. K.; De, M.; Joag, D. S.; More, M. A.; Dravid, V. P. Enhanced Field-Emission Behavior of Layered MoS_2 Sheets. *Small* **2013**, *9*, 2730−2734.

(17) Late, D. J.; Liu, B.; Luo, J. J.; Yan, A. M.; Matte, H. S. S. R.; Grayson, M.; Rao, C. N. R.; Dravid, V. P. GaS and GaSe Ultrathin Layer Transistors. *Adv. Mater.* **2012**, *24*, 3549−3554.

(18) Fang, H.; Chuang, S.; Chang, T. C.; Takei, K.; Takahashi, T.; Javey, A. High-Performance Single Layered WSe_2 p-FETs with Chemically Doped Contacts. *Nano Lett.* **2012**, *12*, 3788−3792.

(19) Liu, W.; Kang, J. H.; Sarkar, D.; Khatami, Y.; Jena, D.; Banerjee, K. Role of Metal Contacts in Designing High-Performance Monolayer n-Type WSe_2 Field Effect Transistors. *Nano Lett.* **2013**, *13*, 1983−1990.

(20) Late, D. J.; Liu, B.; Matte, H.; Rao, C.; Dravid, V. P. Rapid Characterization of Ultrathin Layers of Chalcogenides on SiO_2/Si Substrates. *Adv.Fun. Mater.* **2012**, *22*, 1894−1905.

(21) Rout, C. S.; Joshi, P. D.; Kashid, R. V.; Joag, D. S.; More, M. A.; Simbeck, A. J.; Washington, M.; Nayak, S. K.; Late, D. J. Superior Field Emission Properties of Layered WS_2-RGO Nanocomposites. *Sci. Rep.* **2013**, *3*, 3282.

(22) Dolui, K.; Rungger, I.; Das Pemmaraju, C.; Sanvito, S. Possible Doping Strategies for MoS_2 Monolayers: An Ab Initio Study. *Phys. Rev. B* **2013**, *88*, 1−9.
(23) Eda, G.; Yamaguchi, H.; Voiry, D.; Fujita, T.; Chen, M. W.; Chhowalla, M. Photoluminescence from Chemically Exfoliated MoS_2. *Nano Lett.* **2012**, *12*, 526−526.
(24) Splendiani, A.; Sun, L.; Zhang, Y. B.; Li, T. S.; Kim, J.; Chim, C. Y.; Galli, G.; Wang, F. Emerging Photoluminescence in Monolayer MoS_2. *Nano Lett.* **2010**, *10*, 1271−1275.
(25) Han, S.; Kwon, H.; Kim, S. K.; Ryu, S.; Yun, W. S.; Kim, D.; Hwang, J.; Kang, J.-S.; Baik, J.; Shin, H. Band-Gap Transition Induced by Interlayer Van Der Waals Interaction in MoS_2. *Phys. Rev. B* **2011**, *84*, 045409.
(26) Li, H.; Yin, Z.; He, Q.; Li, H.; Huang, X.; Lu, G.; Fam, D. W. H.; Tok, A. I. Y.; Zhang, Q.; Zhang, H. Fabrication of Single-and Multilayer MoS_2 Film-Based Field-Effect Transistors for Sensing NO at Room Temperature. *Small* **2012**, *8*, 63−67.
(27) Kuc, A.; Zibouche, N.; Heine, T. Influence of Quantum Confinement on the Electronic Structure of the Transition Metal Sulfide TS2. *Phys. Rev. B* **2011**, *83*, 245213.
(28) Li, T. S.; Galli, G. L. Electronic Properties of MOS_2 Nanoparticles. *J. Phys. Chem. C* **2007**, *111*, 16192−16196.
(29) Lebegue, S.; Eriksson, O. Electronic Structure of Two-Dimensional Crystals from ab initio Theory. *Phys. Rev. B* **2009**, *79*, 115409.
(30) Natori, K. Ballistic Metal-Oxide-Semiconductor Field Effect Transistor. *J. Appl. Phys.* **1994**, *76*, 4879−4890.
(31) Chhowalla, M.; Shin, H. S.; Eda, G.; Li, L.-J.; Loh, K. P.; Zhang, H. The Chemistry of Two-Timensional Layered Transition Metal Dichalcogenide Nanosheets. *Nat. Chem.* **2013**, *5*, 263−275.
(32) Huang, X.; Zeng, Z.; Zhang, H. Metal Dichalcogenide Nanosheets: Preparation, Properties and Applications. *Chem. Soc. Rev.* **2013**, *42*, 1934−1946.
(33) Hu, P. A.; Wen, Z. Z.; Wang, L. F.; Tan, P. H.; Xiao, K. Synthesis of Few-Layer GaSe Nanosheets for High Performance Photodetectors. *ACS Nano* **2012**, *6*, 5988−5994.
(34) Late, D. J.; Shaikh, P. A.; Khare, R.; Kashid, R. V.; Chaudhary, M.; More, M. A.; Ogale, S. B. Pulsed Laser-Deposited MoS_2 Thin Films on W and Si: Field Emission and Photoresponse Studies. *ACS Appl. Mater. Interfaces* **2014**, *6*, 15881−15888.
(35) Fan, S. W.; Srivastava, A. K.; Dravid, V. P. Nanopatterned Polycrystalline ZnO for Room Temperature Gas Sensing. *Sens. Actuators, B* **2010**, *144*, 159−163.
(36) Korotcenkov, G. Metal Oxides for Solid-State Gas Sensors: What Determines our Choice? *Mater. Sci. Eng., B* **2007**, *139*, 1−23.
(37) Doll, T.; Lechner, J.; Eisele, I.; Schierbaum, K. D.; Gopel, W. Ozone Detection in the ppb Range with Work function Sensors Operating at Room Temperature. *Sens. Actuators, B* **1996**, *34*, 506−510.
(38) Zhang, W. J.; Huang, J. K.; Chen, C. H.; Chang, Y. H.; Cheng, Y. J.; Li, L. J. High-Gain Phototransistors Based on a CVD MoS_2 Monolayer. *Adv. Mater.* **2013**, *25*, 3456−3461.
(39) Choi, W.; Cho, M. Y.; Konar, A.; Lee, J. H.; Cha, G. B.; Hong, S. C.; Kim, S.; Kim, J.; Jena, D.; Joo, J.; Kim, S. High-Detectivity Multilayer MoS_2 Phototransistors with Spectral Response from Ultraviolet to Infrared. *Adv. Mater.* **2012**, *24*, 5832−5836.
(40) Lee, H. S.; Min, S.-W.; Chang, Y.-G.; Park, M. K.; Nam, T.; Kim, H.; Kim, J. H.; Ryu, S.; Im, S. MoS_2 Nanosheet Phototransistors with Thickness-Modulated Optical Energy Gap. *Nano Lett.* **2012**, *12*, 3695−3700.
(41) Lopez-Sanchez, O.; Lembke, D.; Kayci, M.; Radenovic, A.; Kis, A. Ultrasensitive Photodetectors Based on Monolayer MoS_2. *Nat. Nanotechnol.* **2013**, *8*, 497−501.
(42) Lu, J.; Lu, J.; Liu, H.; Liu, B.; Chan, X. K.; Lin, J.; Chen, W.; Loh, K. P.; Sow, C. H. Improved Photoelectrical Properties of MoS_2 Films after Laser Micromachining. *ACS Nano* **2014**, *8*, 6334−6343.
(43) Li, H.; Yin, Z. Y.; He, Q. Y.; Li, H.; Huang, X.; Lu, G.; Fam, D. W. H.; Tok, A. I. Y.; Zhang, Q.; Zhang, H. Fabrication of Single- and Multilayer MoS_2 Film-Based Field-Effect Transistors for Sensing NO at Room Temperature. *Small* **2012**, *8*, 63−67.
(44) He, Q. Y.; Zeng, Z. Y.; Yin, Z. Y.; Li, H.; Wu, S. X.; Huang, X.; Zhang, H. Fabrication of Flexible MoS_2 Thin-Film Transistor Arrays for Practical Gas-Sensing Applications. *Small* **2012**, *8*, 2994−2999.
(45) Perkins, F. K.; Friedman, A. L.; Cobas, E.; Campbell, P.; Jernigan, G.; Jonker, B. T. Chemical Vapor Sensing with Monolayer MoS_2. *Nano Lett.* **2013**, *13*, 668−673.
(46) Novoselov, K.; Jiang, D.; Schedin, F.; Booth, T.; Khotkevich, V.; Morozov, S.; Geim, A. Two-Dimensional Atomic Crystals. *Proc. Natl. Acad. Sci. U.S.A.* **2005**, *102*, 10451−10453.
(47) Lee, C.; Yan, H.; Brus, L. E.; Heinz, T. F.; Hone, J.; Ryu, S. Anomalous Lattice Vibrations of Single- and Few-Layer MoS_2. *ACS Nano* **2010**, *4*, 2695−2700.
(48) Thripuranthaka, M.; Late, D. J. Temperature Dependent Phonon Shifts in Single-Layer WS2. *ACS Appl. Mater. Interface* **2014**, *6*, 1158−1163.
(49) Late, D. J.; Shirodkar, S. N.; Waghmare, U. V.; Dravid, V. P.; Rao, C. N. R. Thermal Expansion, Anharmonicity and Temperature-Dependent Raman Spectra of Single- and Few-Layer $MoSe_2$ and WSe_2. *ChemPhysChem* **2014**, *15*, 1592−1598.
(50) Ellis, J. K.; Lucero, M. J.; Scuseria, G. E., The Indirect to Direct Band Gap Transition in Multilayered MoS_2 as Predicted by Screened Hybrid Density Functional Theory. *Appl. Phys. Lett.* **2011**, *99*, .
(51) Kuc, A.; Zibouche, N.; Heine, T. Influence of Quantum Confinement on the Electronic Structure of the Transition Metal Sulfide TS_2. *Phys. Rev. B* **2011**, *83*, 245213.
(52) Castellanos-Gomez, A.; Roldan, R.; Cappelluti, E.; Buscema, M.; Guinea, F.; van der Zant, H. S. J.; Steele, G. A. Local Strain Engineering in Atomically Thin MoS_2. *Nano Lett.* **2013**, *13*, 5361−5366.
(53) Yan, R. S.; Simpson, J. R.; Bertolazzi, S.; Brivio, J.; Watson, M.; Wu, X. F.; Kis, A.; Luo, T. F.; Walker, A. R. H.; Xing, H. G. Thermal Conductivity of Monolayer Molybdenum Disulfide Obtained from Temperature-Dependent Raman Spectroscopy. *ACS Nano* **2014**, *8*, 986−993.
(54) Du, Y. C.; Liu, H.; Neal, A. T.; Si, M. W.; Ye, P. D. Molecular Doping of Multilayer MoS_2 Field-Effect Transistors: Reduction in Sheet and Contact Resistances. *IEEE Electron. Device Lett.* **2013**, *34*, 1328−1330.
(55) Thripuranthaka, M.; Kashid, R. V.; Rout, C. S.; Late, D. J. Temperature Dependent Raman Spectroscopy of Chemically Derived Few Layer MoS_2 and WS_2 Nanosheets. *Appl. Phys. Lett.* **2014**, *104*, 081911.
(56) Li, H.; Zhang, Q.; Yap, C. C. R.; Tay, B. K.; Edwin, T. H. T.; Olivier, A.; Baillargeat, D. From Bulk to Monolayer MoS_2: Evolution of Raman Scattering. *Adv. Funct. Mater.* **2012**, *22*, 1385−1390.
(57) Hu, P. A.; Wang, L. F.; Yoon, M.; Zhang, J.; Feng, W.; Wang, X. N.; Wen, Z. Z.; Idrobo, J. C.; Miyamoto, Y.; Geohegan, D. B.; Xiao, K. Highly Responsive Ultrathin GaS Nanosheet. *Nano Lett.* **2013**, *13*, 1649−1654.
(58) Hu, P.; Zhang, J.; Yoon, M.; Qiao, X.-F.; Zhang, X.; Feng, W.; Tan, P.; Zheng, W.; Liu, J.; Wang, X. Highly Sensitive Phototransistors Based on Two-Dimensional GaTe Nanosheets with Direct Bandgap. *Nano Res.* **2014**, *7*, 694−703.
(59) Reemts, J.; Kittel, A. Persistent Photoconductivity in Highly Porous ZnO Films. *J. Appl. Phys.* **2007**, *101*, 013709.
(60) Late, D. J.; Huang, Y. K.; Liu, B.; Acharya, J.; Shirodkar, S. N.; Luo, J. J.; Yan, A. M.; Charles, D.; Waghmare, U. V.; Dravid, V. P.; Rao, C. N. R. Sensing Behavior of Atomically Thin-Layered MoS_2 Transistors. *ACS Nano* **2013**, *7*, 4879−4891.
(61) Liu, B.; Chen, L.; Liu, G.; Abbas, A. N.; Fathi, M.; Zhou, C. High-Performance Chemical Sensing Using Schottky-Contacted Chemical Vapor Deposition Grown Monolayer MoS_2 Transistors. *ACS Nano* **2014**, *8*, 5304−5314.